Gas-Phase Hydration of U(IV), U(V), and U(VI) Dioxo Monocations

Garold L. Gresham,[†] Anita K. Gianotto,[†] Peter de B. Harrington,[‡] Libo Cao,[‡] Jill R. Scott,[†] John E. Olson,[†] Anthony D. Appelhans,[†] Michael J. Van Stipdonk,[§] and Gary. S. Groenewold*,[†]

Idaho National Engineering and Environmental Laboratory, Idaho Falls, Idaho 83415-2208, Center for Intelligent Chemical Instrumentation, Department of Chemistry and Biochemistry, Ohio University, Athens, Ohio 45701-2979, and Department of Chemistry, Wichita State University, Wichita, Kansas

Received: May 24, 2003; In Final Form: July 21, 2003

The formation of adduct ions consisting of uranium oxycations and water was studied using an ion trap-secondary ion mass spectrometer. The U(IV) and U(V) species $[UO(OH)]^+$ and $[UO_2]^+$ were produced by bombarding the surface of UO_3 using molecular primary ions, and the U(VI) species $[UO_2(OH)]^+$ was generated by O_2 oxidation of $[UO(OH)]^+$ in the gas phase. All three ions formed H_2O adducts by termolecular association reactions: $[UO(OH)]^+$ (a U(IV) species) added three water molecules, for a total of five ligands; $[UO_2]^+$ (U(V)) added three or four water molecules, for a total of five or six ligands; and $[UO_2(OH)]^+$ (U(VI)) added four water molecules for a total of six ligands. Addition of a seventh ligand was not observed in any of the systems. These analyses showed that the optimum extent of ligation increased with increasing oxidation state of the uranium metal. Hard kinetic models were fit to the time-dependent mass spectral data using adaptive simulated annealing (ASA) to estimate reaction rates and rate constants from kinetic data sets. The values determined were validated using stochastic kinetic modeling and resulted in rate data for all forward and reverse reactions for the ensemble of reactive ions present in the ion trap. A comparison of the forward rate constants of the hydration steps showed that in general, formation of the monohydrates was slow, but that hydration efficiency increased upon addition of the second H_2O. Addition of the third H_2O was less efficient (except in the case of $[UO_2]^+$), and addition of the fourth H_2O was even more inefficient and did not occur at all in the $[UO_2(OH)]^+$ system. Reverse rate constants also decreased with increasing ligation by H_2O, except in the case of $[UO(OH)(H_2O)_4]^+$, which prefers to quickly revert to the trihydrate. These findings indicate that stability of the hydrate complexes $[UO_yH_z(H_2O)_n]^+$ increases with increasing n, until the optimum number of ligands is achieved. The results enable correlation of uranium hydration behavior with oxidation state.

Introduction

Uranium speciation (i.e., the envelope of oxidation states, oxide forms, and ligand complexes in which the element can exist) has been a topic of sustained interest because it influences processes ranging from nuclear fuel reprocessing[1,2] to mobility in the geologic subsurface.[3] Across this wide-ranging panorama of chemistry, one of the most important chemical species is the uranyl dication UO_2^{2+}, which dominates uranium chemistry in solution and on surfaces. The identity and number of equatorial ligands coordinated with UO_2^{2+} can vary significantly. For monodentate ligands such as water, an equatorial coordination number of 5 is common,[4−6] as measured by X-ray absorption fine structure and Raman studies of aqueous uranyl solutions.[7−11] Additional support for five equatorial H_2O ligands has come from ab initio studies, which concluded that five ligands was more stable than either four or six.[12,13] Similar behavior has been observed in other more varied systems: X-ray absorption fine structure studies of uranyl−humic complexes indicated the presence of five equatorial oxygen atoms,[14] and the presence of bidentate ligands such as oxalate or malonate increased the equatorial coordination number to 6.[4,15] On clay surfaces, the equatorial coordination number increased from ∼4.5 to ∼5.5 with increasing uranyl concentration, which was interpreted in terms of uranyl adsorbed to multiple adsorptive sites.[16] In the solid state, equatorial coordination numbers of 4, 5, or 6 are common, although higher numbers usually involve bidentate ligands.[1] For crystalline compounds such as $UO_2(OH)_2$ and UO_2Cl_2, the equatorial coordination number is 4.[1,17] Much less is known about coordination properties of UO_2^+ because of the tendency of this ion to undergo rapid disproportionation to UO_2 and UO_2^{2+} in aqueous solutions.[1,6] U^{4+} tends to form nine- or higher coordinate complexes as a result of its high charge and also functions as a relatively strong acid owing to its propensity to undergo hydrolysis.[1]

Taken together, past research in the condensed phase indicates that the solvent conditions exert great influence over the extent of coordination. This finding motivated examination of hydration behavior in the gas phase where the intrinsic reactivity of the uranium oxycations might be studied in a more reaction-discrete manner. Previous mass spectrometric studies of U^+ and UO^+ emphasized reactivity with organic compounds;[18−20] the general theme that emerged was the tendency of U^+ to form divalent complexes, resulting in dehydrogenation of the ligated organic and production of π-complexes. Similar patterns of alkane dehydrogenation were observed for UO^+.[21] Additionally, the RO−H and R−OH found in alcohols were susceptible to U^+

* Address correspondence to this author. E-mail:gsg@inel.gov.
[†] Idaho National Engineering and Environmental Laboratory.
[‡] Ohio University.
[§] Wichita State University.

10.1021/jp035443e CCC: $25.00
Published on Web 09/11/2003

TABLE 1: Rate Information from Kinetic Evaluation of $UO_yH_z^+$ Species Reacting with H_2O and O_2 in the IT-SIMS

(#) reaction	$k_{forward}$[a]	forward reaction efficiency[b]	$k_{reverse}$[c]
U(IV): reactions of $[UO(OH)]^+$			
(1) $[UO(OH)]^+ + O_2 \rightarrow [UO_2(OH)]^+ + O^\bullet$	2×10^{-10}	30%	n/a
(2) $[UO(OH)]^+ + H_2O \rightleftarrows [UO(OH)(H_2O)]^+$	0.8×10^{-10}	4%	9
(3) $[UO(OH)(H_2O)]^+ + H_2O \rightleftarrows [UO(OH)(H_2O)_2]^+$	2×10^{-10}	9%	2.0
(4) $[UO(OH)(H_2O)_2]^+ + H_2O \rightleftarrows [UO(OH)(H_2O)_3]^+$	0.3×10^{-10}	2.2%	0.14
(5) $[UO(OH)(H_2O)_3]^+ + H_2O \rightleftarrows [UO(OH)(H_2O)_4]^+$	0.3×10^{-10}	1.2%	11
U(V): reactions of $[UO_2]^+$			
(6) $[UO_2]^+ + H_2O \rightleftarrows [UO_2(H_2O)]^+$	0.6×10^{-10}	3%	8
(7) $[UO_2(H_2O)]^+ + H_2O \rightleftarrows [UO_2(H_2O)_2]^+$	3×10^{-10}	15%	15
(8) $[UO_2(H_2O)_2]^+ + H_2O \rightleftarrows [UO_2(H_2O)_3]^+$	4×10^{-10}	19%	2.2
(9) $[UO_2(H_2O)_3]^+ + H_2O \rightleftarrows [UO_2(H_2O)_4]^+$	0.6×10^{-10}	3%	1.7
U(VI): reactions of $[UO_2(OH)]^+$			
(10) $[UO_2(OH)]^+ + H_2O \rightleftarrows [UO_2(OH)(H_2O)]^+$	0.4×10^{-10}	1.9%	1.0
(11) $[UO_2(OH)(H_2O)]^+ + H_2O \rightleftarrows [UO_2(OH)(H_2O)_2]^+$	1×10^{-10}	7.1%	0.8
(12) $[UO_2(OH)(H_2O)_2]^+ + H_2O \rightleftarrows [UO_2(OH)(H_2O)_3]^+$	0.5×10^{-10}	2.2%	0.22

[a] cm^3 $molecule^{-1}$ s^{-1}. [b] Efficiency of $k_{forward}$ as a percentage of k_{ADO} except for (1) where it is expressed as a percentage of $k_{Langevin}$. [c] sec^{-1}.

and UO^+ insertion reactions.[22] In the presence of organic radicals, U^+ had a high affinity for σ-bound dicarbide and acetylide anions.[23]

Oxidation reactions constituted a second category of gas-phase U^+ reactions that have been studied: Armentrout and Beauchamp originally oxidized U^+ using O_2, CO, CO_2, COS, and D_2O,[24] and further studies showed that UO^+ would undergo oxidation with O_2, and D_2O to form UO_2^+.[24] These studies were amplified by Schwarz and co-workers, who showed that rapid oxidation of U^+ and UO^+ would occur using N_2O in addition to O_2.[25] Consistent results for O_2 oxidation of U^+ and UO^+ were reported by Duckworth and co-workers in a study that emphasized reactivity of U^{2+}.[26] More recently, studies by Gibson showed that U^+ could also be oxidized using ethylene oxide.[27] This intriguing envelope of U^+ and UO^+ reactivity enticed the present investigation of more highly oxidized species that bear closer similarity to those encountered under ambient pressure and hydration conditions.

We report here the first examination of the intrinsic hydration reactivity of U(IV), U(V), and U(VI) dioxo monocations, which reveals the kinetics for the formation of the inner hydration sphere. The hydration behavior provides a foundation for understanding more complex solubilization processes critical to uranium behavior in industrial separations and mobility in the geosphere.[28] Additionally, the study provides insight into the behavior of uranium-bearing cations in the gas phase. A quadrupole ion trap-secondary ion mass spectrometer (IT-SIMS) was used to form the uranium oxycations by particle sputtering. The reactant ion of interest was isolated and reacted with gaseous water at modest He pressure that enabled collisional stabilization of more fragile adducts.[29] Control of the time between ion generation and detection enabled reaction pathways and kinetics to be deduced. To compare reactivity among different species, deterministic kinetic models were fit to the time-dependent mass spectral data using a novel adaptive simulated annealing (ASA) approach to estimate reaction rates and rate constants. Stochastic kinetic modeling was used to validate the estimated rate constants. The combined ion trap-kinetic modeling strategy has been used in the authors' laboratory for the study of the reactions of Si, Al, and Cr oxyanions with H_2O,[30−33] H_2S,[34] and O_2.[35,36]

Experimental Section

Gas-Phase Atmosphere of the IT-SIMS. H_2O was admitted to the vacuum chamber after two freeze−pump−thaw cycles to reduce the admittance of dissolved gases. A variable leak valve was then used to control the admittance of H_2O vapor into the IT-SIMS for the ion−molecule reaction experiments. H_2O pressure in the ion−molecule experiments was maintained between 1.2 and 1.4 $\times$ 10^{-6} Torr and was measured using a Bayerd−Alpert ion gauge mounted on the vacuum manifold. Because the ion gauge response for H_2O is nearly identical to N_2,[37] ion gauge pressures were used to calculate H_2O number densities without correction for ion gauge sensitivities.[37] The actual pressure within the ion trap itself could not be measured directly but is probably very close to that in the manifold; we base this statement on the fact that fast reactions were proceeding at the collision limit, but not faster, as calculated using apparent pseudo-first-order kinetic analyses and the H_2O concentration measured using the ion gauge. The ion trap atmosphere also contained residual O_2, which was present in the ion trap as part of the ambient background and as a result of the water addition. The partial pressure of O_2 was between 2 and 3 $\times$ 10^{-7} Torr, which was sufficient to oxidize $[UO(OH)]^+$; hence, an accurate estimate of O_2 concentration was needed. The ion ratio (*m*/*z* 32/total ion) was measured using a residual gas analyzer (Inficon, Syracuse, NY) and then multiplied by the ion gauge reading to determine the partial pressure of O_2. This approach resulted in a value that was consistent with a back calculation of O_2 concentration that was performed by measuring the rate constant for $[UO(OH)]^+ + O_2$ at an O_2 pressure of 1.5 $\times$ 10^{-6} Torr, which resulted in calculation of a rate constant of 2 $\times$ 10^{-10} cm^3 $molecule^{-1}$ s^{-1} (Table 1). This rate constant could be divided into the rate measured at low O_2 partial pressure to generate an O_2 concentration value that agreed with that calculated using the ion ratio approach. After the H_2O (and O_2) were admitted, the He bath gas was added so that the total pressure was 2 $\times$ 10^{-5} Torr (uncorrected); thus, the uncorrected partial pressure of He was approximately 1.8 $\times$ 10^{-5} Torr, or 9 $\times$ 10^{-5} Torr corrected for ion gauge sensitivity.[37] The IT-SIMS base pressure was typically 5 $\times$ 10^{-8} Torr.

Gas-phase $[UO_yH_z]^+$ species were produced by bombarding powdered Uranium (VI) oxide (Strem Chemicals, Newburyport, MA) attached to the end of a 2.7-mm probe tip using self-assembly adhesive (3M, St. Paul, MN). The sputtered $[UO_yH_z]^+$ ions were then trapped in the IT-SIMS, where they were subsequently reacted with the gaseous H_2O and O_2.

Ion−Molecule Reactions in the IT-SIMS. The instrument used in this study was based on a modified Varian Saturn 2000

ITMS (Walnut Creek, CA) previously described in the literature.[38−40] The instrument was equipped with a ReO_4^- primary ion beam that is more efficient for sputtering cluster ions into the gas phase relative to atomic particle bombardment.[41−44] The ReO_4^- ion gun is mounted collinear with the axis of the ion trap and the beam enters the ion trap through an aperture in the top end cap. The beam passes along the main axis of the ion trap and strikes the sample located behind the opposite end cap. The ReO_4^- ion gun was operated at 5.0 keV, at a primary ion current of ~700 picoamps measured using a Faraday cup.

The ReO_4^- beam was gated to only impact the sample during the ionization period of the IT-SIMS analysis sequence. Ionization times were adjusted to produce sufficient secondary ions to conduct the reactivity studies at an acceptable signal-to-noise level. The typical ionization time for the $[UO_2]^+ + H_2O$ reactivity studies was 5 ms, and typical ionization times of 50 and 45 ms were used, respectively, for the $[UO(OH)]^+/[UO_2(OH)]^+ + H_2O$ reactivity studies. Secondary ions sputtered from the sample surface were focused into the ion trap using a small cylindrical electrostatic lens, which also served to mitigate charge buildup on the bombarded sample surface.[45] During the ionization period, the reactant ions of interest ($[UO_2]^+$ and $[UO(OH)]^+$) were isolated using selected ion storage,[46] which resulted in ejection of unwanted ions on the basis of their mass-dependent motional frequencies. Isolated ions were then allowed to react with H_2O during a specified reaction time (0−2 s) that was systematically controlled. Because no doubly charged ions were produced by ReO_4^- bombardment of the sample, the ion trap was operated at a low mass cutoff of 160 amu during the ionization and reaction time periods. Finally, the ionic reactants and products were scanned out of the trap[46] and deflected onto a venetian blind dynode positioned in front of the multichannel plate detector, located off axis between the end of the ion trap and the primary ion gun. A diagram of the instrument can be found in a previous article.[38]

The time progression of the reactions was observed by varying the specified reaction time and then by recording a mass spectrum. Four spectra were collected at each time interval, which enabled the variability in the relative abundances to be assessed at each time point. Standard deviations in the ion abundances are represented by the error bars found in Figures 3, 5, and 6.

Kinetic Analysis using ASA. Analysis of the kinetic data sets required a robust approach because of the occurrence of simultaneous serial and parallel, forward and reverse reactions. As described in the following paragraphs, reaction pathways were identified using multivariate curve resolution (SIMPLISMA), and the time-dependent mass spectra were decomposed into time-dependent and mass spectral matrixes. Laplace transformation of the matrixes produced kinetic rate equations that were fit to the data using adaptive simulated annealing (ASA).

A multivariate curve resolution approach[47] was employed to identify reaction pathways in an unbiased fashion. The mass spectra for each time measurement were consolidated into a Microsoft Excel spreadsheet and read directly into MATLAB 6.5 (The Mathworks, Inc, Natick, MA). Ion abundances were normalized to the total ion abundance in each spectrum, which corrected for a 10−20% increase that slowly occurs with increasing time. This increase results from kinetic cooling of the ions, which improves their detection efficiency. Reactant and product ion relationships and their general kinetic behavior were determined using the multivariate curve resolution method

SCHEME 1: Forward and Reverse Water Addition Reactions of $[UO_yH_z]^+$ [a]

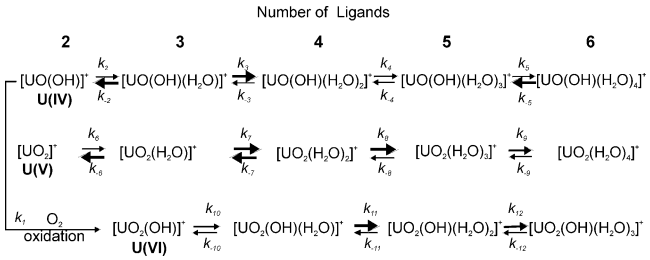

[a] The thickness of the arrows is roughly correlated with the relative magnitude of the rate constants.

SIMPLISMA.[48] SIMPLISMA decomposed the matrix of transient mass spectra into two matrixes. The first matrix comprises ion profiles with respect to time. Each profile corresponds to a different reaction pathway. Ions having the same profile (e.g., isotopic ions) follow parallel reaction pathways. This matrix reveals the overall kinetic behavior and reaction pathways of the experiment. The second matrix comprises mass spectra. Each mass spectrum contains ions that are reacting in parallel. When multiple isotopes are present, the isotopic distribution typically appears in these spectra. Thus, SIMPLISMA is a useful tool for simplifying complex kinetic measurements that comprise parallel reactions.

The coupled temporal behavior of the ions revealed in the two matrixes enabled construction of kinetic models that contained: (a) several sequential reactions in the reaction sequence beginning with $[UO_2]^+$ (Scheme 1, reactions 6 to 9 and −6 to −9), and (b) several sequential reactions along two parallel pathways in the sequence beginning with $[UO(OH)]^+$ (reactions 1−5, −2 to −5, 10−12, and −10 to −12). The Laplace transformation of the matrixes was used to derive the integrated kinetic rate equations. The equations were obtained using Cramer's rule and evaluating symbolic determinants with MATLAB 6.5 and the Symbolic Toolbox. Some of the integrated rate expressions were over 60 pages of a typical word document in length or 30 000 characters per line of the MATLAB script. The basic approach was outlined by Andraos.[49]

Adaptive simulated annealing (ASA)[50,51] was used to fit these intricate equations to the data because of its benefits over other methods such as genetic algorithms.[52] The ASA version 24.2 C source was MEXX compiled under MATLAB 6.5. A MATLAB interface ASAMIN version 1.24 was used to call the MEXX routines in MATLAB. The following parameters were changed from the default so as to achieve precise rate constant estimates: temperature ratio scale = 1.0×10^{-10}; limit generated = 1.0×10^6; limit acceptances = 1.0×10^4. The average CPU times for the optimizations of *m*/*z* 270 in excess H_2O and *m*/*z* 271 in excess H_2O and in excess O_2 were 39, 21, and 18 min. The differences in optimization times corresponded to the complexity of the integrated kinetic model.

The key ion channels (i.e., *m*/*z* channels) were culled from the data set and normalized so that at each time measurement the sum of the ion intensities totaled to unity. The objective function for the ASA algorithm minimized the sum of the squares of the differences between integrated rate expression and the normalized MS data. The calculations were performed on an AMD XP 1700+ processor equipped 512 MB of PC266 MHz RAM operating under MS Windows XP Pro SP1. Each evaluation used five different randomized starting conditions for the ASA optimization. The output of this approach was explicit rate constants for all reactions in the kinetic model. For

simplicity in discussion, we refer to the overall approach as "ASA".

The rate constants reported were generated by fitting all data in aggregate. The RMS error (i.e., difference between the model and the data) for each of the 15 ion profiles was <0.022, and the total residual error was random and $\leq 4\%$. To assess precision, the data points were grouped into twenty, randomly assembled time progressions (bootstrapped data sets), which were fitted to the kinetic model using ASA as outlined above. The average relative standard deviation (rsd) for the rate constants (k) for the U(V) hydration series (starting from $[UO_2]^+$) was 30%. The average rsd for the k values for the U(IV) and U(VI) hydration series (starting from $[UO(OH)]^+$) was 58%. The larger average rsd reflected additional uncertainty resulting from more degrees of freedom in the kinetic model (15 reactions starting from $[UO(OH)]^+$ versus only 8 starting from $[UO_2]^+$). The imprecision from the bootstrapped data sets motivated independent model validation, which was performed using a stochastic approach.

Stochastic Validation of the Kinetic Models. The reaction progressions determined using ASA were then modeled using a stochastic kinetic modeling approach based on a rigorously derived Monte Carlo procedure that numerically simulated the time evolution of the reactions involved.[53,54] The stochastic kinetic modeling was performed using the Chemical Kinetic Simulator software package, that is available for a no-cost license on the IBM website.[55] The input for the modeling was the rate information generated using ASA (summarized in Table 1) and the neutral H_2O and O_2 number densities derived from the partial pressure measurements, divided by 1000 to accommodate numerical limitations in the software. $[H_2O]$ used for modeling the reactions starting from $[UO_2]^+$ was 3.58×10^7 molecules cm^{-3}. For reactions starting from $[UO(OH)]^+$, $[H_2O] = 4.44 \times 10^7$ and $[O_2] = 8.7 \times 10^6$ molecules cm^{-3}. At the end of the modeling, the 1000 division was corrected by dividing the time axis by 1000 prior to plotting. The number density used for the reactant ions was 1000 molecules cm^{-3}. Previous ion molecule kinetics research demonstrated equivalency of the stochastic kinetic simulations with rigorous deterministic kinetic models.[34]

Reaction Efficiency. Reaction efficiency was evaluated by comparing forward rate constants from the fitted kinetic analyses with theoretical rate constants calculated using the reparametrized average-dipole-orientation (ADO) theory.[56] The reparametrized ADO constants were calculated using a reaction temperature (310 K), which was the average ion temperature for an ion in a typical trap as calculated by Goeringer and McLuckey,[57] and Gronert.[58] The efficiency of the O_2 oxidation (reaction 1) was compared with the Langevin collision constant.[59] The actual temperature of the ions is unknown, and the results of the reaction chemistry studies showed that the ions were energetically above the temperature of the He bath gas, both as a result of the low He pressure in the IT-SIMS and as a result of the exothermicity of the hydration reactions. However, we have no reason to believe that the ions were substantially above the energy of typical ions in a quadrupole ion trap because organic ions that normally do not survive the SIMS ionization process are observed as stable ions, and in addition the reparametrized ADO constant is not acutely sensitive to increased temperature.

Results and Discussion

Secondary Ion Mass Spectrum of Uranium (VI) Oxide. The cation SIMS spectrum of UO_3 collected using an IT-SIMS

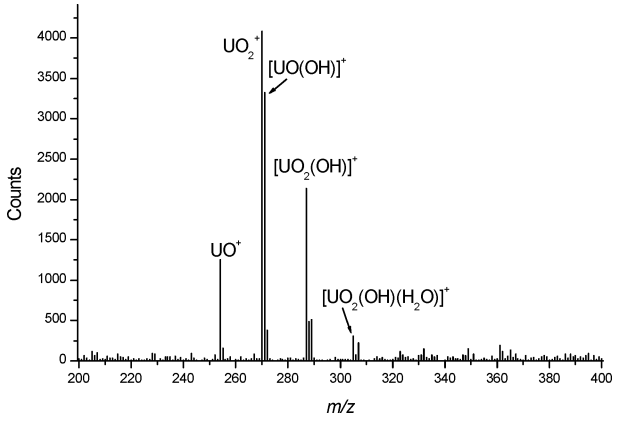

Figure 1. Cation IT-SIMS spectra of UO_3. Observed ions originate from SIMS sputtering and also from reaction with background water and oxygen present in the atmosphere of the ion trap.

(Figure 1) contained abundant ions formally corresponding to U oxycations where U is formally in the III, IV, V, and VI oxidation states. The ion at m/z 254 is $[UO]^+$ (U(III)), which underwent oxidation to form $[UO_2]^+$ (m/z 270, U(V)) and $[UO(OH)]^+$ (m/z 271, U(IV)) as previously reported.[24] In the ion isolation experiments, however, most of the $[UO_2]^+$ and $[UO(OH)]^+$ were formed directly from surface bombardment. A low abundance ion at m/z 272 may be accounted for by formation of a $[UO(H_2O)]^+$ adduct, but this was not a prominent process when UO^+ was isolated, and hence the ion may be derived from direct formation of $[U(OH)_2]^+$. The peak at m/z 287 is $[UO_2(OH)]^+$ (U(VI)), which is formed directly by sputtering, and also by oxidation of $[UO(OH)]^+$. No $[UO_2]^{2+}$ was observed in the IT-SIMS spectrum, which precluded investigation of this ion.

Low abundance ions observed at m/z 288, 289, 305, 306, and 307 were identified as H_2O adducts formed from reactions of the U oxycations with residual H_2O that was present in the IT-SIMS. The H_2O adducts afforded the opportunity to study the intrinsic hydration chemistry of U oxycations in the IV, V, and VI oxidation states. The ion isolation process eliminated virtually all contributions from neighboring reactants which enabled determination of reaction pathways and kinetics. These are presented in order of increasing oxidation state in the following sections.

Reactions of the U(IV) Oxycation $[UO(OH)]^+$. A controlled H_2O concentration was established in the IT-SIMS, after which m/z 271 $[UO(OH)]^+$ was produced by sputtering and then isolated. Spectra were recorded at increasing time intervals, which showed the temporal evolution of pairs of ions that were separated by two amu (Figure 2). The lower mass ion series at m/z 287, 305, 323, and 341 was initiated by oxidation of $[UO(OH)]^+$ by residual O_2 that was present in the ion trap (reaction 1, see Table 1, and Scheme 1 for reactions), and produced $[UO_2(OH)]^+$ at m/z 287. This reaction pathway was verified by addition of excess O_2 to the IT-SIMS, and the bimolecular rate constant (k_1) was calculated at 2×10^{-10} cm^3 $molecule^{-1}$ s^{-1}, which was $\sim$28% efficient compared with the Langevin collision constant.[59] $[UO_2(OH)]^+$ (a U(VI) species) underwent three hydration steps to produce m/z 305, 323, and 341 (vide infra). In the high He pressure in the IT, the oxidation and hydration reactions are certainly termolecular;[60,61] activated $[UO_yH_z(O_2)]^+$ and $[UO_yH_z(H_2O)_n]^+$ complexes are stabilized by collisions with He.[29] The explicit effect of the He could not be evaluated effectively over the range of operational pressures in the IT-SIMS, but previous studies conducted in our lab on metal oxide anions did not demonstrate significant changes in reaction

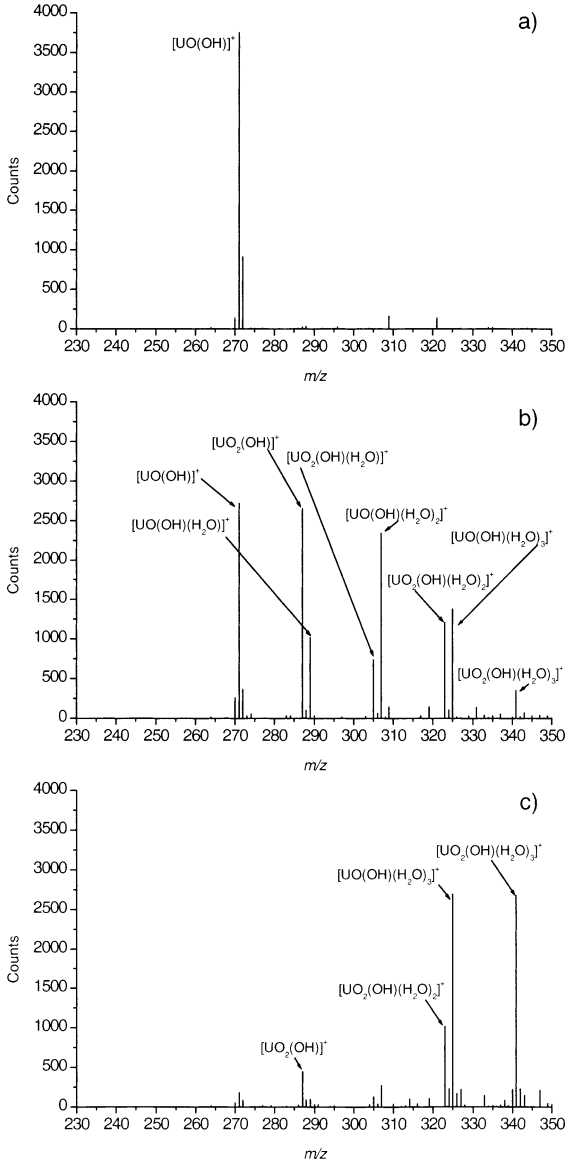

Figure 2. IT-SIMS spectra acquired after isolation of $[UO(OH)]^+$ (*m*/*z* 271) with H_2O pressure of 1.4×10^{-6} Torr. Reaction times of (a) 0 s, (b) 0.60 s, and (c) 2.00 s.

rates over our range of operational He pressures. This limitation notwithstanding, the reactions could be reasonably modeled as effective bimolecular processes,[62] which provides a basis for comparison.

The hydration reactions of $[UO_2(OH)]^+$ proceeded in parallel with hydration reactions of the U(IV) species $[UO(OH)]^+$, which formed H_2O adducts at *m*/*z* 289, 307, 325, and 343. An important observation was that there was no interconversion between the parallel hydration series starting from $[UO(OH)]^+$ (U(IV)) and $[UO_2(OH)]^+$ (U(VI)) after the first hydration step. Isolation and reaction of $[UO(OH)(H_2O)]^+$ produced no ions containing oxidized U, which indicated that once hydrated, oxidation of $[UO(OH)]^+$ was inhibited. Further, $[UO_2(OH)]^+$ bearing species were not reduced: isolation of $[UO_2(OH)(H_2O)]^+$ did not produce U(IV)-bearing ions during subsequent reactions with water or by collision-induced dissociation.

The kinetic behavior was evaluated by plotting the ion abundances of $[UO(OH)]^+$ and its hydrated adducts versus time (Figure 3). The appearance of this plot was consistent with a model that incorporated four forward and four reverse reactions (reactions 2−5, forward and reverse, Scheme 1, Table 1). To

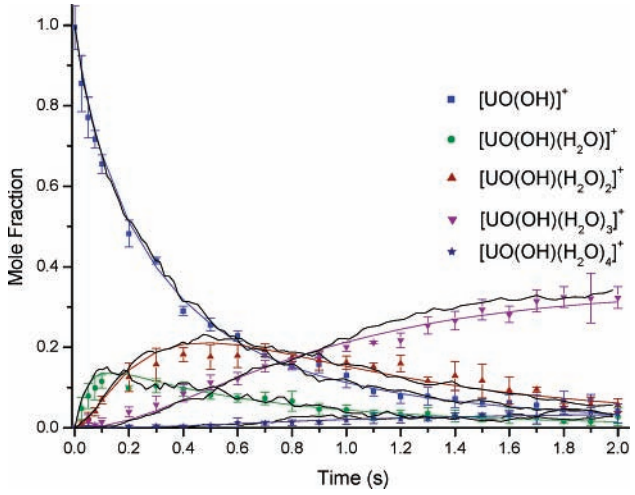

Figure 3. Kinetic plot of ion abundance versus time for the hydration reactions of $[UO(OH)]^+$ occurring in 1.4×10^{-6} Torr H_2O. Filled symbols with error bars are data from the IT-SIMS. Smooth colored lines are extracted kinetic profiles generated using ASA kinetic modeling. Irregular black lines were generated using stochastic kinetic simulation. Note that these hydration reactions were occurring in parallel with the oxidation and hydration reactions represented in Figure 6, and consequently the product ion abundances at any given time in this plot do not equal the initial reactant ion concentration. Fractional ion abundances in Figure 3 and Figure 6 sum to one at any given time.

extract the individual reaction rates of the eight serial hydration/dehydration reactions of $[UO(OH)]^+$ (which were occurring in parallel with the oxidation and six additional reactions stemming from $[UO_2(OH)]^+$, see Figure 6), adaptive simulated annealing (ASA, see Experimental Section) was utilized to fit the data to the reaction model. The reverse reactions were required to kinetically model the data, that is, kinetic plots that even remotely resembled the data could not be generated using only forward reactions (the exception to this was the irreversible O_2 oxidation of $[UO(OH)]^+$). Plots of the temporal behavior of the ion abundances generated using ASA were in good agreement with the data (Figure 3). To validate the ASA treatment, the rate constants and concentrations of H_2O and O_2 values were used as input for a stochastic kinetic simulation. The results of the stochastic model were also in good agreement with the data as well as the ASA method. The coincidence of the data, the ASA kinetic analysis, and the stochastic modeling encouraged an examination of reactivity trends.

The U(IV) species $[UO(OH)]^+$ underwent initial hydration (reaction 2) only grudgingly (4% efficient), and kinetic modeling showed that the product ion $[UO(OH)(H_2O)]^+$ at *m*/*z* 289 reverted to the precursor ion at *m*/*z* 271 at a much faster rate. To evaluate the reverse reaction, $[UO(OH)(H_2O)]^+$ was isolated, whereupon only further forward reactions with H_2O were observed, and the reverse reaction was not observed without mild collision-induced dissociation. This indicated that $[UO(OH)(H_2O)]^+$ is initially formed as a species activated to dissociate but is stabilized over the course of time through collisions with the IT-SIMS atmosphere. The reverse reaction is not observed in the experiment where $[UO(OH)(H_2O)]^+$ is isolated because only stable species survive the isolation step, which requires time, resulting in additional vibrational thermalization. This finding indicated that the whole ensemble of ions is to some extent hyperthermal, with extra energy either residual from the desorption event (kinetic or vibrational) or from exothermicity of the hydration step. A potentially more elegant means to measure rate constants would be to isolate stabilized individual hydrate molecules; however, this was

beyond the instrument control capabilities of the IT-SIMS because it would require multiple isolation/reaction steps. The alternative was to adopt the present approach, in which a single reactant ion was isolated and the multiple-step hydration process was allowed to cascade forward. While energetically less explicit, the kinetic analysis of the experiments resulted in individual forward and reverse rate constants, which provided insight into the formation of the initial hydration sphere occurring dynamically in the quadrupole ion trap.

The variable behavior of the *m*/*z* 289 ion may be due to two different structures. $[UO(OH)(H_2O)]^+$ may be initially formed and may undergo rearrangement to $[U(OH)_3]^+$, which may be in part responsible for the increasing stability with time in the trap. The rearrangement would be an intramolecular analogue to well-known hydrolysis reactions of U(IV) species that occur in solution,[6] but distinguishing between these two structural possibilities is beyond the ability of the experiment.

The second hydration step, in which $[UO(OH)(H_2O)_2]^+$ at *m*/*z* 307 is formed (reaction 3), is more than twice as fast as the initial hydration step. The larger rate constant for the addition of the second H_2O ligand ($k_3 > k_2$) indicates that the monohydrate is more reactive than the initial reactant ion $[UO(OH)]^+$, which is reminiscent of the behavior of AlO_2^-, in which the addition of the second H_2O molecule was substantially faster than the addition of the first.[30] Changes in the electron density of the acceptor orbitals or in the dipole moment of the reactant ion may be responsible for this behavior; in fact, a very low ion dipole was suggested to account for very low reactivity of AlO_2^-.[30] The observation that the rate of the reverse reaction is slower for $[UO(OH)(H_2O)_2]^+$ than for $[UO(OH)(H_2O)]^+$ ($k_{-3} < k_{-2}$) indicates that the dihydrate is more stable, which might be due to intraligand H-bonding. However, indications from preliminary ab initio calculations suggest that the directionality of the lone pairs on the water molecules does not lend itself to the formation of stabilizing hydrogen bonding, at least in the lowest energy conformations. Detailed ab initio calculations currently underway may shed some light on the kinetic influence of intramolecular hydrogen bonding, alterations in the electron density within acceptor orbitals, and the dipole moment of the uranyl ion.[63]

The rate of formation of the trihydrate $[UO(OH)(H_2O)_3]^+$ (reaction 4) was slower, perhaps reflecting some repulsion by the previously bound ligands. However, the rate of the reverse reaction was even slower yet, which strongly favored formation of the trihydrate, and suggested higher stability for $[UO(OH)(H_2O)_3]^+$. Formation of the tetrahydrate $[UO(OH)(H_2O)_4]^+$ (reaction 5) occurred but was not preferred; it underwent fast dissociation back to the trihydrate. There was no evidence for addition of a fifth H_2O. On the basis of the rate constants and mass spectra, it is clear that most of the ions prefer to exist as the trihydrate (Figure 3), which indicates that 5 is the preferred coordination number for water complexes of $[UO(OH)]^+$ in the gas phase.

Reactions of the U(V) Oxycation $[UO_2]^+$. The U(V) species $[UO_2]^+$ at *m*/*z* 270 reacted with H_2O to form $[UO_2(H_2O)_n]^+$, where $1 \leq n \leq 4$, which resulted from serial addition of H_2O molecules to $[UO_2]^+$ (reactions 6−9, Figure 4, Scheme 1). A conceptual kinetic model employing four forward and four reverse reactions enabled accurate simulation of the time-dependent $[UO_2]^+$ hydration data. Extraction of rates using ASA and validation using stochastic modeling resulted in graphical superimposition of the data, the ASA plots, and the stochastic simulation (Figure 5). As in $[UO(OH)]^+$, the coincidence of the data and the results from the two modeling approaches encouraged comparison of ion reactivities and stabilities.

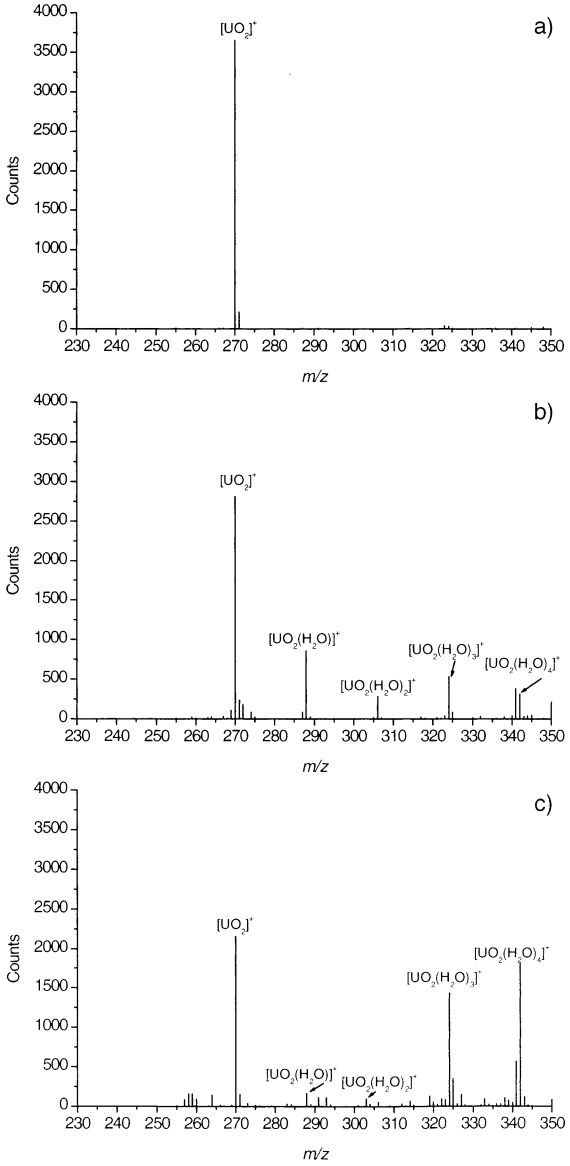

Figure 4. IT-SIMS spectra acquired after isolation of $[UO_2]^+$ (*m*/*z* 270) with H_2O pressure of 1.2×10^{-6} Torr. Reaction times of (a) 0 s, (b) 0.50 s, and (c) 2.00 s.

The hydration behavior of $[UO_2]^{2+}$ was similar to that of $[UO(OH)]^+$ in that the first hydration step (k_6) was slow and was accompanied by a fast back reaction (large k_{-6}). Addition of the second H_2O to form the $[UO_2]^+$ dihydrate was much faster (reaction 7), but the very large k_{-7} indicated that the dihydrate was relatively unstable, and principally favored dissociation. However in addition to being unstable, the dihydrate was also highly reactive toward addition of a third H_2O (reaction 8); k_8 was nearly 20% of the ADO collision constant and was the fastest of the hydration reactions in this study. The reverse reaction (dissociation of the trihydrate) was slow (small k_{-8} value), and hence at intermediate times (~0.8 s, Figure 5), $[UO_2(H_2O)_3]^+$ is the dominant product ion.

Formation of the tetrahydrate (reaction 9) $[UO_2(H_2O)_4]^+$ was significantly slower than the preceding two hydration steps, but the reverse reaction was also slow (small k_{-9} value), and thus the tetrahydrate was the most abundant product ion at the longest reaction times accessible in the IT-SIMS. At longer reaction times, most of the ion abundance would be concentrated in the

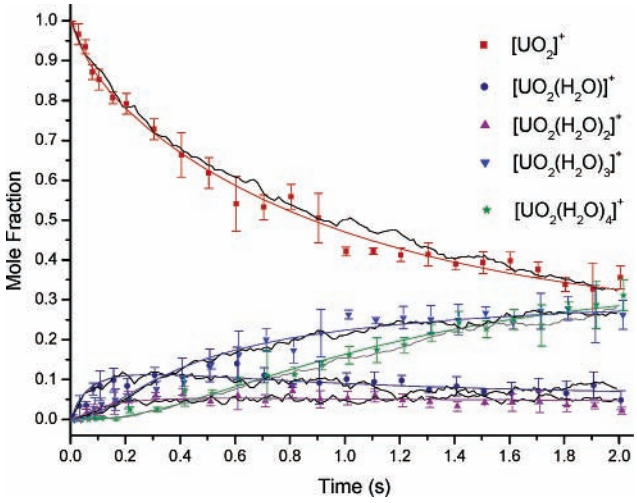

Figure 5. Kinetic plot of ion abundance versus time for the hydration reactions of $[UO_2]^+$ occurring in 1.2×10^{-6} Torr H_2O. Filled symbols with error bars are data from the IT-SIMS. Smooth colored lines are extracted kinetic profiles generated using ASA kinetic modeling. Irregular black lines were generated using stochastic kinetic simulation.

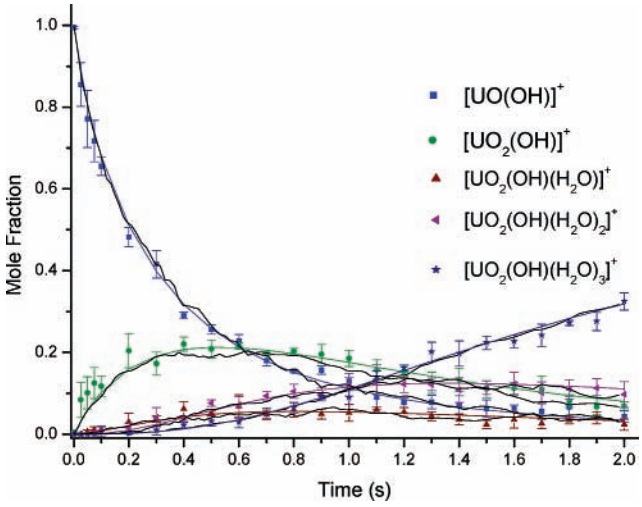

Figure 6. Kinetic plot of ion abundance versus time for $[UO(OH)]^+$ reacting with 2.8×10^{-7} Torr O_2 to form $[UO_2(OH)]^+$, which then reacts with 1.4×10^{-6} Torr H_2O to form mono-, di-, and trihydrates. Filled symbols with error bars are data from the IT-SIMS. Smooth colored lines are extracted kinetic profiles generated using ASA kinetic modeling. Irregular black lines were generated using stochastic kinetic simulation. Note that these oxidation/hydration reactions were occurring in parallel with the hydration reactions represented in Figure 3, and consequently the product ion abundances at any given time in this plot do not equal the initial reactant ion concentration. Fractional ion abundances in this Figure and Figure 3 sum to one at any given time.

tetrahydrate, but the trihydrate may remain competitive to some extent. There was no evidence for formation of a $[UO_2(H_2O)_5]^+$, which suggests that a coordination number of 6 is preferred for U(V) monocations under the 10^{-4} Torr He environment of the IT-SIMS.

Reactions of the U(VI) Oxycation $[UO_2(OH)]^+$. As noted in the section on U(IV), the sputtered ion $[UO(OH)]^+$ was oxidized by residual O_2 in the ion trap to form the U(VI) species $[UO_2(OH)]^+$. The structure of the molecule is unknown, with protonated, trigonal $[UO_3(H)]^+$ one possibility, and a hydroxy−uranyl ion pair $[UO_2(OH)]^+$, with the hydroxide anion occupying an equatorial coordination site being a second. In the condensed phases, there is substantial evidence for the latter, particularly given the pronounced tendency for the UO_2^{2+} to undergo hydrolysis in solution,[1] which forms the hydroxy−uranyl ion pair. Here, the hydroxy ligand is unlikely to perturb the very strong uranyl bonds, which are usually considered to be U≡O with a formal charge of 3.3 on U (favoring a linear O−U−O geometry). Our preference for the latter structure was further supported by observation of the same ion formed using electrospray ionization (ESI) of an aqueous uranyl solution:[64] the hydration behavior was identical in both the ESI and IT-SIMS experiments, strongly indicating equivalence. Formation of an ion having a $[UO_3(H)]^+$ structure in the ESI experiment would be difficult to rationalize starting from a UO_2^{2+} solution. For these reasons, we will proceed in describing the *m*/*z* 287 ion as the uranyl−hydroxide ion pair $[UO_2(OH)]^+$, with the acknowledged caveat that other structures are within the realm of possibility.

Upon formation, $[UO_2(OH)]^+$ began reacting with H_2O to form $[UO_2(OH)(H_2O)_n]^+$, where ions in which $1 \le n \le 3$ were observed at *m*/*z* 305, 323, and 341 (Figure 2). Hydrolysis involving the axial oxygen atoms would not be expected, since the uranyl U═O bond is very strong.[1] As in the previous two cases, a kinetic model that incorporated forward *and* reverse reactions enabled numerical kinetic modeling that produced excellent agreement between the data, ion abundances calculated from the ASA-generated rates, and the stochastic simulation (Figure 6).

Addition of the initial H_2O molecule (the second equatorial ligand) was slow (k_{10}, 1.9% efficient) but still faster than the reverse, and hence formation of $[UO_2(OH)(H_2O)]^+$ was favored. The hydroxymonohydrate then added a second H_2O at a faster rate (k_{11}, 7% efficient), and the dissociation reaction was slow, which meant that the formation of the hydroxydihydrate $[UO_2(OH)(H_2O)_2]^+$ was favored over the hydroxymonohydrate. Addition of the third H_2O to form $[UO_2(OH)(H_2O)_3]^+$ was somewhat slower (k_{12}, 2.1% efficient), but once formed, the octahedral $[UO_2(OH)(H_2O)_3]^+$ was very stable, having a practically negligible dissociation rate. There was no evidence for addition of a fourth H_2O ligand to the system, within the reaction time constraints of the IT-SIMS. If a fourth H_2O is added, the rate constant can be no greater than $\sim 1 \times 10^{-12}$ cm^3 molecule^{-1} s^{-1}, which represents the slowest reactions we can observe in the IT-SIMS. These observations indicated that at longer times, virtually all of the ion abundance in this system would be concentrated in the octahedral hydroxytrihydrate, $[UO_2(OH)(H_2O)_3]^+$, which indicates that 6 is the preferred coordination number for the $[UO_2(OH)]^+$ system.

Extent of $[UO_yH_z]^+$ Coordination. In the gas phase, the extent of coordination of the uranium dioxy monocations increases from five to six as the formal oxidation state of U increases from IV to V to VI. This suggests that increased electron density in the valence molecular orbitals of the U(IV) (and to a lesser degree the U(V)) species repels addition of a sixth ligand and implies that interactions with incoming H_2O molecules involve the O lone pairs. The repulsion is strongest in the most reduced species $[UO(OH)]^+$, which clearly prefers only five ligands. Repulsion would be less pronounced for the U(V) species $[UO_2]^+$, in which case five- and six-ligand complexes are competitive at the longest time scales accessible in the IT-SIMS.

The U(VI) species $[UO_2(OH)]^+$ most probably adheres to a uranyl structural motif and hence has empty δ_u and ϕ_u molecular orbitals (predominantly derived from *f* atomic orbitals)[65] that are responsible for equatorial coordination of three additional H_2O, for a preferred coordination number of 6. The results indicate a correlation between the oxidation state of the U atom in the complexes and the extent of coordination of the uranium

oxomonocations in the modest vacuum environment of the quadrupole ion trap.

Comparative Ion Reactivity. The generation of explicit forward rate constants enabled qualitative evaluation of reactivity as a function of extent of coordination and oxidation state. For $[UO(OH)]^+$, $[UO_2]^+$, and $[UO_2(OH)]^+$, additions of the first H_2O molecule were slow processes, being only 2−4% efficient, and emphasize the need for collisional stabilization of the monohydrates (consistent with large reverse rate constants for the U(IV) and U(V) systems). The lack of a pronounced dipole *in the ion* may discourage proper orientation of the incoming H_2O as it approaches the oxycations. However, a better explanation may be that there are insufficient vibrational modes to accommodate reaction exothermicity, and a more explicit approach will be required to evaluate this hypothesis.

Addition of the second H_2O was significantly faster in each case, indicating that the monohydrates are more reactive than the unhydrated cations. In contrast to the unhydrated cations, the monohydrates may have a more significant dipole moment and would have additional degrees of freedom, both of which would be expected to increase reaction efficiency.

The oxidation state of the oxycations appears to strongly influence the addition of the third H_2O. For the U(IV) cation $[UO(OH)(H_2O)_2]^+$, addition of the third H_2O is markedly slower than addition of the second H_2O, perhaps reflecting electronic repulsion. In contrast, addition of the third H_2O to the U(V) cation $[UO_2(H_2O)_2]^+$ is very efficient, which might reflect availability of unfilled low-lying bonding orbitals. In the U(VI) species $[UO_2(OH)(H_2O)_2]^+$, addition of the third H_2O is considerably slowed; this reactant ion already contains three equatorial ligands, and we hypothesize that steric crowding may be responsible for decreased reaction efficiency.

Addition of a fourth H_2O is noticeably slowed for both the U(IV) and U(V) oxycation systems (and does not occur at all for the U(VI) system). The fourth H_2O addition represents the sixth ligand in both cases, and we have already seen that addition of the sixth ligand is substantially slower in the U(VI) system.

Ion Stability Trends. The reverse reaction rate constants were compared to evaluate relative ion stabilities. The U(IV) and U(V) monohydrates dissociated at fast rates, indicating low stability of the initially formed complexes; in contrast the dissociation constant (k_{-10}) for the U(VI) monohydrate $[UO_2(OH)(H_2O)]^+$ was quite a bit smaller. In this latter case, the $[UO_2(OH)]^+$ may be better able to accommodate the reaction energy of the first hydration step.

Dissociation rates of the U(IV) and U(VI) dihydrates were modest, which is in keeping with the general trend of increasing ion stability with increasing hydration. However, the U(V) species $[UO_2(H_2O)_2]^+$ is a notable exception, in that it has a very large dissociation constant (k_{-7}). The origin of this large rate constant is unknown. Dissociation rates of the trihydrates were significantly less than the dihydrates in each case, which indicates that as H_2O addition proceeds, the hydrated U oxycations become progressively more stable. In the U(IV) species $[UO(OH)(H_2O)_3]^+$ and the U(VI) species $[UO_2(OH)(H_2O)_3]^+$, the dissociation rates were negligibly small, indicating a high level of stability for these complexes.

The U(V) system also becomes more stable upon addition of a fourth H_2O, which corresponds to the sixth ligand, although stability difference is not as pronounced as in the U(VI) case: the dissociation rate constant for $[UO_2(H_2O)_4]^+$ is 8 times greater than that for the corresponding $[UO_2(OH)(H_2O)_3]^+$. In contrast, the U(IV) complex $[UO(OH)(H_2O)_4]^+$ is unstable, with a large dissociation rate constant k_{-5} indicating that its preferred ligand number has been exceeded.

Acknowledgment. This research was supported by the United States Department of Energy Environmental Systems Research Program under contract DE-AC-07-99ID13727 BBWI. M.V.S. acknowledges support from the Kansas NSF EPSCoR program and the Kansas Technology Enterprise Corporation through a First Award. P.B.H. acknowledges support from the Research Corporation Research Opportunity Award, The Idaho National Engineering and Environmental Laboratory Faculty Fellowship, and the Ohio University Faculty Fellowship Leave. He also thanks Lester Ingber for advice pertaining to ASA.

References and Notes

(1) Greenwood, N. N.; Earnshaw, A. *Chemistry of the Elements*, 2nd ed.; Butterworth Heinemann: Oxford, Great Britain, 1997.
(2) Schulz, W. W.; Navratil, J. D. *Science and Technology of Tributyl Phosphate*; CRC Press: Boca Raton, FL, 1984.
(3) Brookins, D. G. *Geochemical Aspects of Radioactive Waste Disposal*; Springer-Verlag: New York, 1984.
(4) Meinrath, G. *J. Radioanal. Nucl. Chem.* **1996**, *211*, 349−362.
(5) Evans, H. T. *Science* **1963**, *141*, 154−158.
(6) Rizkalla, E. N.; Choppin, G. R. Lanthanides and Actinides Hydration and Hydrolysis. In *Handbook on the Physics and Chemistry of Rare Earths;* Gschneidner, Jr., K. A., Eyring, L., Choppin, G. R., Lander, G. H., Eds.; Lanthanides/Actinides: Chemistry, Vol. 18; North-Holland: New York, 1994; pp 529−558.
(7) Thompson, H. A.; Brown, G. E.; Parks, G. A. *Am. Miner.* **1997**, *82*, 483−496.
(8) Aberg, M.; Ferri, D.; Glaser, J.; Grenthe, I. *Inorg. Chem.* **1983**, *22*, 3986−3989.
(9) Allen, P. G.; Bucher, J. J.; Shuh, D. K.; Edelstein, N. M.; Reich, T. *Inorg. Chem.* **1997**, *36*, 4676−4683.
(10) Dent, A. J.; Ramsay, J. D. F.; Swanton, S. W. *J. Colloid Interface Sci.* **1992**, *150*, 45−60.
(11) Nguyen-Trung, C.; Palmer, D. A.; Begun, G. M.; Peiffert, C.; Mesmer, R. E. *J. Solution Chem.* **2000**, *29*, 101−129.
(12) Clavaguera-Sarrio, C.; Brenner, V.; Hoyau, S.; Marsden, C. J.; Millie, P.; Dognon, J.-P. *J. Phys. Chem., B* **2003**, *107*, 3051−3060.
(13) Spencer, S.; Gagliardi, L.; Handy, N. C.; Ioannou, A. G.; Skylaris, C.-K.; Willetts, A.; Simper, A. M. *J. Phys. Chem., A* **1999**, *103*, 1831−1837.
(14) Denicke, M. A.; Pompe, S.; Reich, T.; Moll, H.; Bubner, M.; Heise, K. H.; Nocolai, R.; Nitsche, H. *Radiochim. Acta* **1997**, *79*, 151−160.
(15) Jiang, J.; Rao, L.; Clark, S. B.; Di Bernardo, P.; Zanonato, P.; Bismondo, A. Temperature effects on the actinide complexation with carboxylate ligands; Pacifichem, Honolulu, HI, 2000.
(16) Chisholm-Brause, C.; Conradson, S. D.; Buscher, C. T.; Eller, P. G.; Morris, D. E. *Geochim. Cosmochim. Acta* **1994**, *58*, 3625−3631.
(17) Roof, R. B.; Cromer, D. T.; Larson, A. C. *Acta Crystallogr.* **1964**, *17*, 701.
(18) Gibson, J. K. *Int. J. Mass Spectrom. Ion Processes* **2002**, *213*, 1.
(19) Heinemann, C.; Cornehl, H. H.; Schwarz, H. *J. Organomet. Chem.* **1995**, *501*, 201−209.
(20) Gibson, J. K. *Organometallics* **1997**, *16*, 4214−4222.
(21) Gibson, J. K. *J. Am. Chem. Soc.* **1998**, *120*, 2633−2640.
(22) Gibson, J. K. *J. Mass Spectrom.* **1999**, *34*, 1166−1177.
(23) Gibson, J. K. *J. Vac. Sci. Technol., A* **1997**, *15*, 2107−2118.
(24) Armentrout, P. B.; Beauchamp, J. L. *Chem. Phys.* **1980**, *50*, 27−36.
(25) Cornehl, H. H.; Heinemann, C.; Marcalo, J.; de Matos, A. P.; Schwarz, H. *Angew. Chem., Int. Ed. Engl.* **1996**, *35*, 891−894.
(26) Jackson, G. P.; King, F. L.; Goeringer, D. E.; Duckworth, D. C. *J. Phys. Chem., A* **2002**, *106*, 7788−7794.
(27) Gibson, J. K. *J. Mass Spectrom.* **2001**, *36*, 284−293.
(28) Murphy, W. M.; Schock, E. L. Environmental Aqueous Geochemistry of Actinides. In *Uranium: Mineralogy, Geochemistry and the Environment*; Burns, P. C., Finch, R., Eds.; Mineralogical Society of America: Washington, D. C., 1999; Vol. 38, pp 221−254.
(29) Brodbelt, J. S. Effects of Collisional Cooling on Ion Detection. In *Practical Aspects of Ion Trap Mass Spectrometry*; March, R. E., Todd, J. F. J., Eds.; CRC Press: New York, 1995; pp 209−220.
(30) Scott, J. R.; Groenewold, G. S.; Gianotto, A. K.; Benson, M. T.; Wright, J. B. *J. Phys. Chem., A* **2000**, *104*, 7079−90.
(31) Groenewold, G. S.; Scott, J. R.; Gianotto, A. K.; Hodges, B. D. M.; Kessinger, G. F.; Benson, M. T.; Wright, J. B. *J. Phys. Chem., A* **2001**, *105*, 9681−9688.

(32) Gianotto, A. K.; Hodges, B. D. M.; Benson, M.; Harrington, P. B.; Appelhans, A. D.; Olson, J. E.; Groenewold, G. S. *J. Phys. Chem. A* **2003**, *107*, 5948−5955.
(33) Groenewold, G. S.; Kessinger, G. F.; Scott, J. R.; Gianotto, A. K.; Appelhans, A. D.; Delmore, J. E.; Avci, R. *Anal. Chem.* **2001**, *73*, 226−232.
(34) Groenewold, G. S.; Hodges, B. D. M.; Scott, J. R.; Gianotto, A. K.; Appelhans, A. D.; Kessinger, G. F.; Wright, J. B. *J. Phys. Chem., A* **2001**, *105*, 4059−4064.
(35) Gianotto, A. K.; Hodges, B. D. M.; Harrington, P. B.; Appelhans, A. D.; Olson, J. E.; Groenewold, G. S. *J. Am. Soc. Mass Spectrom.* **2003**, *14*, in press.
(36) Gianotto, A. K.; Hodges, B. S. M.; Appelhans, A. D.; Groenewold, G. S.; Benson, M. T. *J. Am. Soc. Mass Spectrom.* **2002**, *13*, 87S, ThPQ 360.
(37) Bartmess, J. E.; Georgiadis, R. M. *Vacuum* **1983**, *33*, 149−153.
(38) Gresham, G. L.; Groenewold, G. S.; Olson, J. E. *J. Mass Spectrom.* **2000**, *35*, 1460−1469.
(39) Groenewold, G. S.; Appelhans, A. D.; Ingram, J. C.; Gresham, G. L.; Gianotto, A. K. *Talanta* **1998**, *47*, 981−986.
(40) Groenewold, G. S.; Appelhans, A. D.; Ingram, J. C. *J. Am. Soc. Mass Spectrom.* **1998**, *9*, 35−41.
(41) Appelhans, A. D.; Delmore, J. E. *Anal. Chem.* **1989**, *61*, 1087−1093.
(42) Van Stipdonk, M. J.; Justes, D. R.; Santiago, V.; Schweikert, E. A. *Rapid Commun. Mass Spectrom.* **1998**, *12*, 1639−1643.
(43) Harris, R. D.; Van Stipdonk, M. J.; Schweikert, E. A. *Int. J. Mass Spectrom.* **1998**, *174*, 167−177.
(44) Groenewold, G. S.; Delmore, J. E.; Olson, J. E.; Appelhans, A. D.; Ingram, J. C.; Dahl, D. A. *Int. J. Mass Spectrom. Ion Processes* **1997**, *163*, 185−195.
(45) Dahl, D. A.; Appelhans, A. D. *Int. J. Mass Spectrom.* **1998**, *178*, 187−204.
(46) *Practical Aspects of Ion Trap Mass Spectrometry*; Todd, J. F. J., Ed.; CRC Press: New York, 1995; Vol. 1, p 4.
(47) Harrington, P. B.; Gianotto, A. K.; Hodges, B. D. M.; Groenewold, G. S. **2002**, in preparation.
(48) Windig, W.; Guilment, J. *Anal. Chem.* **1991**, *63*, 1425−1432.
(49) Andraos, J. A. *J. Chem. Educ.* **1999**, *76*, 1578−1583.
(50) Ingber, L. *Mathematical Computer Modelling* **1993**, *18*, 29−57.
(51) Ingber, L. Global optimization C-code Adaptive Simulated Annealing (ASA); Caltech Alumni Association, 1993.
(52) Ingber, L.; Rosen, B. *Mathematical Computer Modelling* **1992**, *16*, 87−100.
(53) Gillespie, D. T. *J. Comput. Phys.* **1976**, *22*, 403−34.
(54) Gillespie, D. T. *J. Phys. Chem.* **1977**, *81*, 2340−2362.
(55) Hinsberg, W. D.; Houle, F. A. Chemical Kinetics Simulator v.1.01 The program package, including supporting documentation, is available for a no-cost license from IBM at http://www.almaden.ibm.com/st/msim/. A reference for the basic algorithm is Gillespie, D. J. *J. Comput. Phys.* **1976**, *22*, 403.
(56) Su, T.; Chesnavich, W. J. *J. Chem. Phys.* **1982**, *76*, 5183−5185.
(57) Goeringer, D. E.; McLuckey, S. A. *Int. J. Mass Spectrom. Ion Processes* **1998**, *177*, 163−174.
(58) Gronert, S. *J. Am. Soc. Mass Spectrom.* **1998**, *9*, 845−848.
(59) Gioumousis, T.; Stevenson, D. P. *J. Chem. Phys.* **1958**, *29*, 294.
(60) Peschke, M.; Blades, A. T.; Kebarle, P. *J. Phys. Chem., A* **1998**, *102*, 9978−9985.
(61) Jayaweera, P.; Blades, A. T.; ikonomou, M. G.; Kebarle, P. *J. Am. Chem. Soc.* **1990**, *112*, 2452−2454.
(62) Weishaar, J. C. *Acc. Chem. Res.* **1993**, *26*, 213−219.
(63) Van Stipdonk, M. J. Unpublished results, 2003.
(64) Hanna, D.; Anbalagan, V.; Gresham, G. L.; Groenewold, G. S.; Van Stipdonk, M. J. *J. Am. Soc. Mass Spectrom.* **2003**, in press.
(65) Denning, R. G. *Struct. Bonding* **1992**, *79*, 215−276.